Energy 196 (2020) 117065

Contents lists available at ScienceDirect

Energy

journal homepage: www.elsevier.com/locate/energy

Quantification of parameter uncertainty in wind farm wake modeling

Jincheng Zhang, Xiaowei Zhao*

School of Engineering, University of Warwick, CV4 7AL, Coventry, UK

ARTICLE INFO

Article history:
Received 14 November 2019
Received in revised form
16 January 2020
Accepted 28 January 2020
Available online 1 February 2020

Keywords:
Uncertainty quantification
Wake modeling
Bayesian inference
Wind farm simulations

ABSTRACT

Reliable prediction of wind turbine wakes is essential for the optimal design and operation of wind farms. In order to achieve this, the parameter uncertainty of analytical wake model is investigated for the first time. Specifically, large eddy simulations (LES) of wind farms are carried out with different turbine yaw angles, based on SOWFA (Simulator fOr Wind Farm Applications) platform. The generated high-fidelity flow field data is used to infer the low-fidelity model's parameters within the Bayesian uncertainty quantification framework. After model calibration, the posterior model check shows that the predicted mean velocity profile with the quantified uncertainty matches well with the high-fidelity CFD data. The prediction of other quantities, such as wind farm flow field and turbine power generation, is also carried out. The results show that the wake model with the model parameters specified by their posterior distributions can be seen as the stochastic extension of the original wake model. As most of the existing wake models are static, the resulting stochastic model shows a great advantage over the original model, as it can give not only the static wind farm properties but also their statistical distributions.

1. Introduction

As one of the most important clean energy resources, wind energy has been investigated extensively all over the world. In order to reduce the overall cost of wind power harvesting, wind turbines are usually grouped together to form a large wind farm. However, wake interactions between individual turbines within a wind farm have a large impact on the farm's overall performance [1], e.g., the wind turbines operating in the wakes caused by the upstream turbines usually generate less electricity and experience more severe structural load due to the reduced wind speed and increased flow turbulence. Therefore, wake modeling is of great importance in order to take wake interactions into account in the optimal design and control of wind farms, which is becoming a very active area [2,3]. A range of wake models have been developed in the literature [4], including the high-fidelity large eddy simulation (LES) models [5,6], medium-fidelity 2D dynamic models [7,8], and low-fidelity analytical models [9–11].

The high-fidelity models solve the Navier-Stokes equation with the turbine rotor represented by actuator lines [12–14] or actuator disks [15–18]. Despite the rapid development of high-performance computing technology, the high-fidelity models are still not suitable for the control design or real-time control study due to their high computational cost and long simulation time. Thus the low-fidelity wake models based on analytical formulations [19–21] remain the main tool in the industry and are still under active development [22–25]. However, these models are not able to precisely predict the detailed flow dynamics and careful calibration of empirical model parameters is often needed to increase the prediction accuracy [26]. The underlying uncertainty of analytical wake models needs to be investigated in order to achieve reliable predictions of wind turbine wakes.

The input uncertainty and model uncertainty are the two main sources of uncertainty in wind turbine wake predictions. The former has been investigated in the literature. In Ref. [27], wind direction uncertainty was investigated and its impact on predicting turbine power generation was evaluated. The results showed the inclusion of direction uncertainty improved the agreement between the power predictions of analytical wake models and measurement data. In Ref. [28], Jensen wake model was employed with the consideration of the inflow direction uncertainty to predict the wake profile behind wind turbines and the results showed a better match between the predicted wake profiles and measurement data. Recently, the inclusion of uncertainty in active wake control is also receiving attention [29,30]. However, all these work only considered the input uncertainty and did not consider the model uncertainty. The inclusion of model uncertainty is of great importance for

* Corresponding author.
E-mail addresses: jincheng.zhang@warwick.ac.uk (J. Zhang), xiaowei.zhao@warwick.ac.uk (X. Zhao).

https://doi.org/10.1016/j.energy.2020.117065
0360-5442/

Table 1
The prior range of model parameters.

Model parameter	k_d	a_d	b_d	k_e	$m_{e,1}$	$m_{e,2}$	$m_{e,3}$	a_U	b_U	$M_{U,1}$	$M_{U,2}$	$M_{U,3}$
Left boundary	0.05	−50.0	−0.05	0.04	−1.0	−0.3	0.0	0.0	0.66	0.2	0.7	3.0
Right boundary	0.25	50.0	0.05	0.14	−0.2	0.3	4.0	10.0	2.66	0.8	1.3	15.0

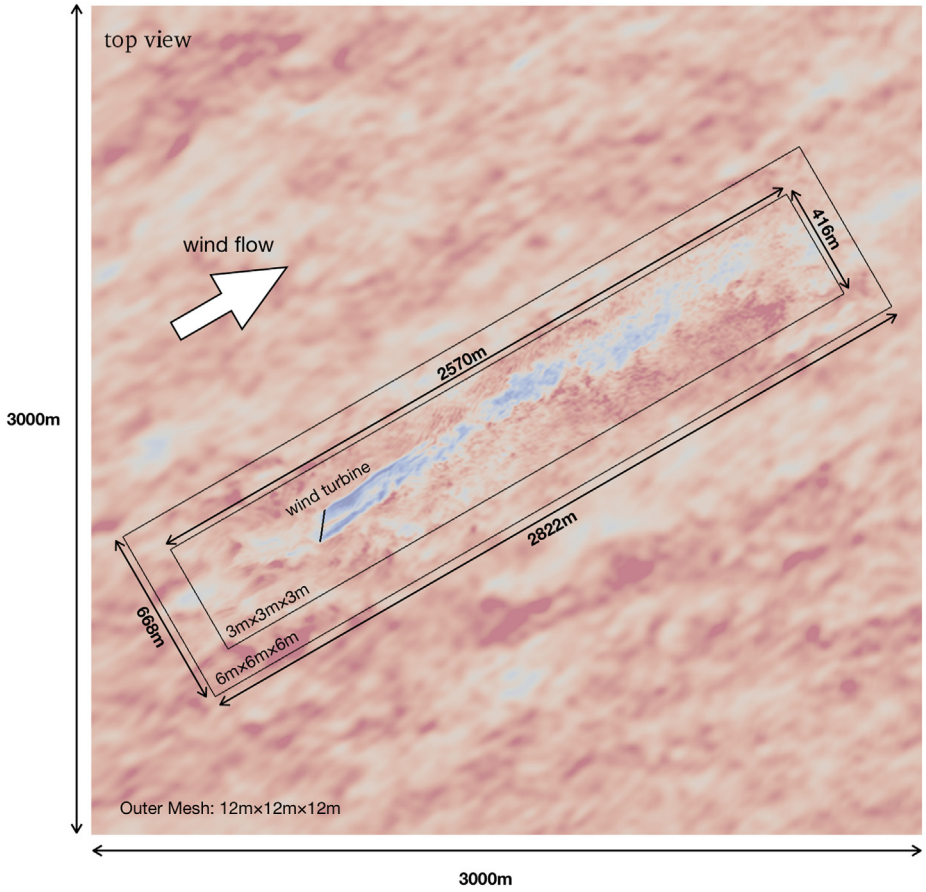

Fig. 1. A top view of the simulation domain at turbine hub height. The contour shows the instantaneous flow field at 400s for the case with turbine yaw angle γ equal to $-$ 40°.

reliable predictions of wind turbine wakes, which enables optimal design and control of wind farm. Therefore, the present paper focuses on rigorously quantifying the model uncertainty in wind farm wake predictions in the Bayesian uncertainty quantification (UQ) framework.

The Bayesian UQ for a general computer model was first presented by Kennedy and O'Hagan [31], where the model uncertainty was classified into parameter uncertainty, model inadequacy, residual variability, parametric uncertainty, code uncertainty, etc. Among them, the parameter uncertainty and model inadequacy are the two most important uncertainty sources. The former arises from the lack of knowledge of the heuristic model parameters and the latter represents the discrepancy between the true physical values and the model output at the optimal model parameters. In recent years, a lot of research attention has been paid to the parameter uncertainty of fluid dynamics such as boundary layer flows [32–34], channel flows [35], transitional flows [36], compressible jet-in-crossflow [37], etc. To our knowledge, the parameter uncertainty of wake model in wind farm simulations has not been investigated yet in the literature, which is the main aim of the present paper. The advantage of capturing model uncertainty through model parameters instead of model inadequacy is that the former allows the multi-turbine predictions with quantified uncertainty being carried out in a straightforward manner.

The empirical parameters in existing data-driven analytical wake modeling [14,38] were usually calibrated against high-fidelity simulations or measurement data. But the underlying uncertainty was usually ignored in these work thus only fixed-point predictions can be carried out for the quantities of interest (QoIs). In the present work, the high-fidelity LES data, here generated by SOWFA (Simulator for Onshore/Offshore Wind Farm Applications) [39,40], is used to calibrate the analytical wake model, using FLORIS (FLOw redirection and Induction in Steady-state) [14] as an example, in terms of the parameters' probability distribution functions (PDFs) in the Bayesian UQ framework. The resulting model with parameter uncertainty (called stochastic FLORIS) can predict the statistics of the QoIs which include the information for both the mean value and the corresponding uncertainty while the fixed-point calibration can only predict a single value. An apparent advantage of this method is that it can be used to not only maximise the average power but also minimise the power fluctuation while the fixed-point prediction of the QoIs cannot be used for the latter.

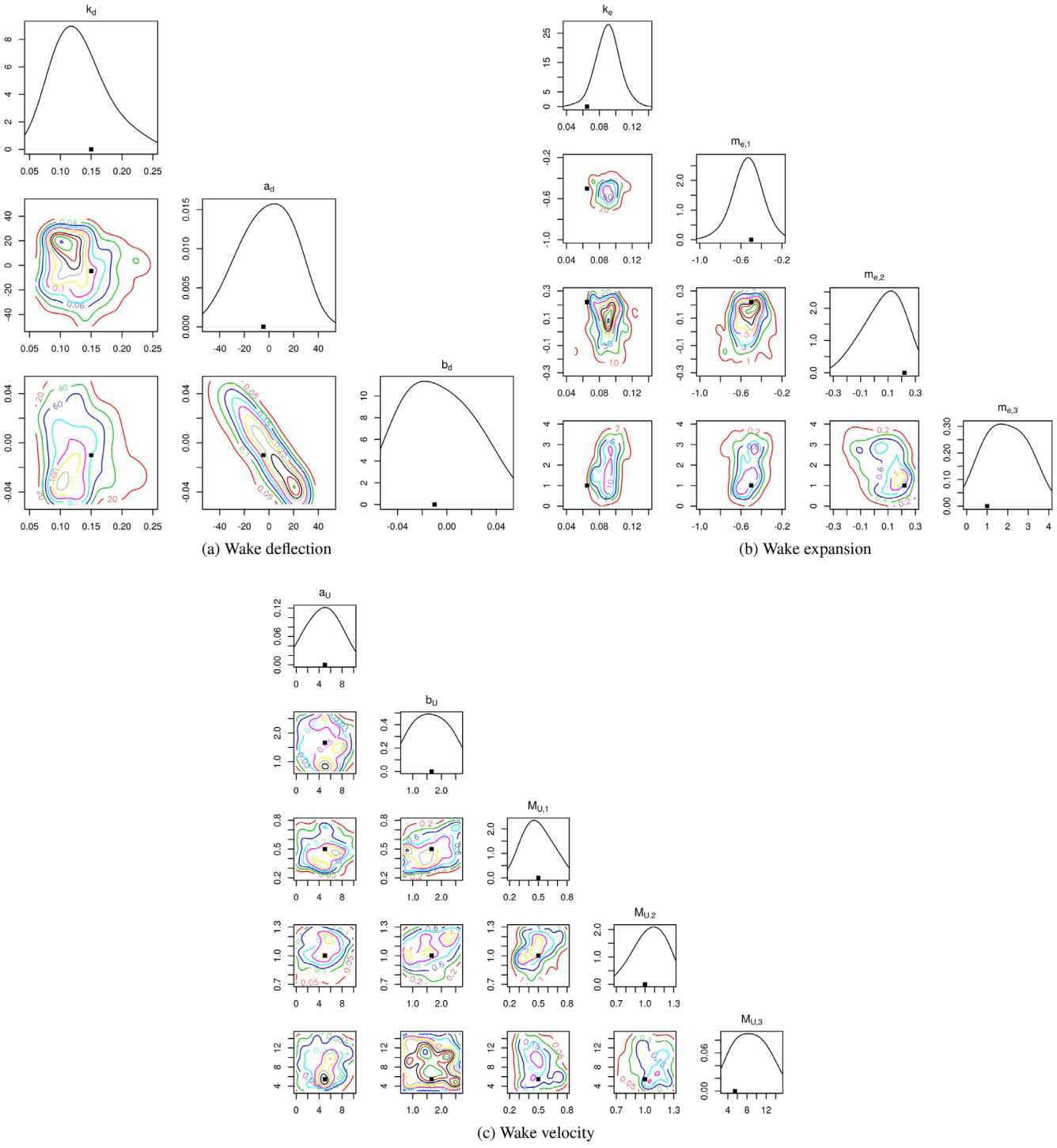

(a) Wake deflection

(b) Wake expansion

(c) Wake velocity

Fig. 2. The posterior distribution of the model parameters arising from modeling wake deflection, wake expansion, and wake velocity. The square points represent the nominal values of the model parameters reported in Ref. [14].

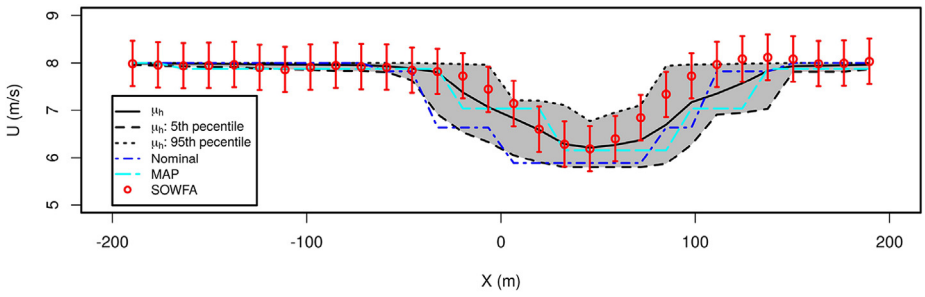

(a) $\gamma = -40°$

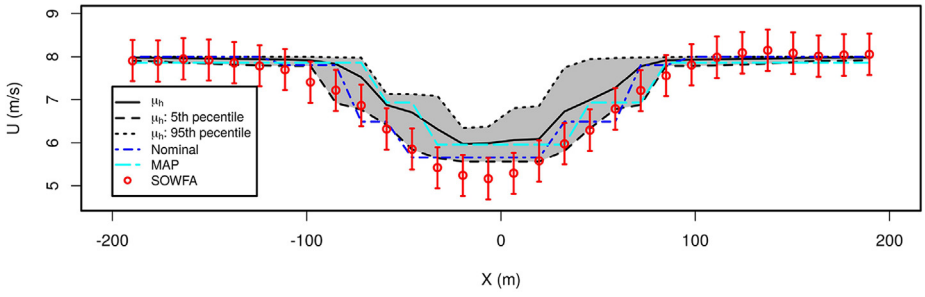

(b) $\gamma = 0°$

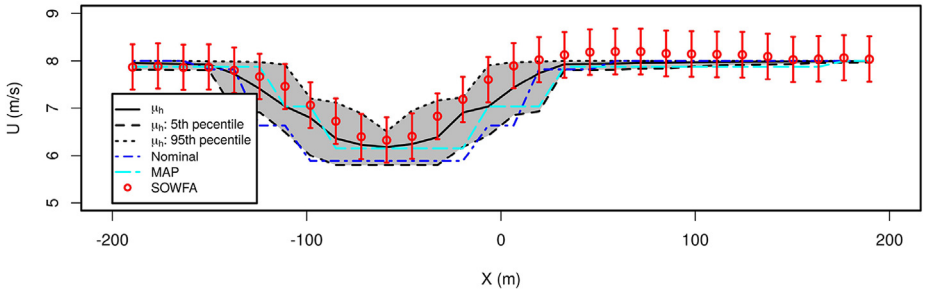

(c) $\gamma = 40°$

Fig. 3. The predictions of the velocity profiles at 5 rotor diameters downstream for three different yaw angles ($\gamma = -40°, 0°, 40°$). The high-fidelity SOWFA results are also included.

Our study shows that the stochastic FLORIS performs much better than the original wake model FLORIS. First, the mean flow field prediction is greatly improved and a correct characteristic of uncertainty in the "mixing zone" is predicted, which agrees with the high-fidelity SOWFA results. Second, the prediction for the power generation shows that the stochastic FLORIS performs similarly as the FLORIS model in terms of predicting average turbine power, but it performs much better in terms of predicting the turbine power fluctuation. The main contribution of the present paper is the first application of uncertainty quantification method in wind farm wake modeling and the detailed analysis of the resulting stochastic model. This work paves the way for wind farm predictions with quantified uncertainty and the proposed framework can be easily applied to other wake models.

The remaining part of this paper is organised as follows: the Bayesian UQ approach is described in Section 2. The application of the UQ approach in the wake model FLORIS is described in Section 3, where the formulation of FLORIS and the procedure of high-fidelity data generation are given. The results are given in Section 4, including the parameter uncertainty of FLORIS inferred from the high-fidelity data and the evaluation of the prediction performance of the developed FLORIS model with parameter uncertainty. The conclusions are drawn in Section 5.

2. Bayesian uncertainty quantification

The UQ approach used in this work is briefly described in this section and further details can be found in Refs. [33,34]. In Bayesian UQ framework, various forms of uncertainties are represented through random variables, which are usually characterized by their PDFs. Here for the parameter uncertainty, model parameters are treated as random variables. According to Bayes' rule, the posterior distributions of model parameters can be obtained by

$$p(\mathbf{z}|\mathbf{d}) \propto p(\mathbf{d}||\mathbf{z})p(\mathbf{z}), \tag{1}$$

where p($\mathbf{z}$) represents the prior distribution of the model parameters $\mathbf{z}$ and p($\mathbf{d}|\mathbf{z}$) represents the likelihood of the experimental observation $\mathbf{d}$ given $\mathbf{z}$. A stochastic model needs to be constructed in order to obtain the likelihood. In this work it is constructed by simply modeling the model inadequacy through a multiplicative

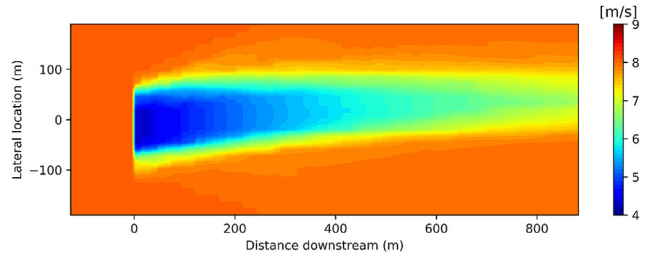

(a) Mean value predicted by stochastic FLORIS

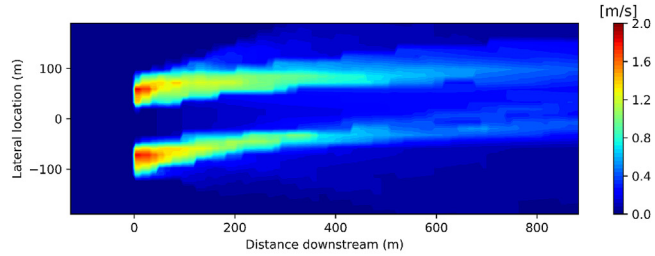

(b) Standard deviation predicted by stochastic FLORIS

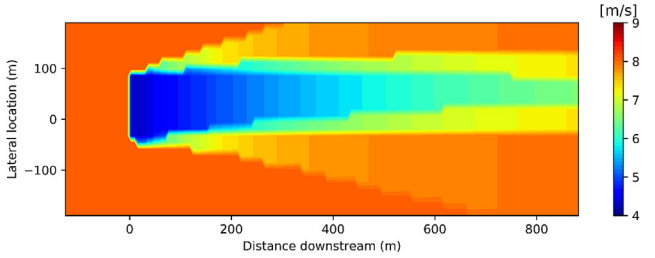

(c) FLORIS with MAP model parameters

Fig. 4. The prediction of the flow field by the stochastic FLORIS model and FLORIS with MAP model parameters, for the case of turbine yaw equal to − 40°.

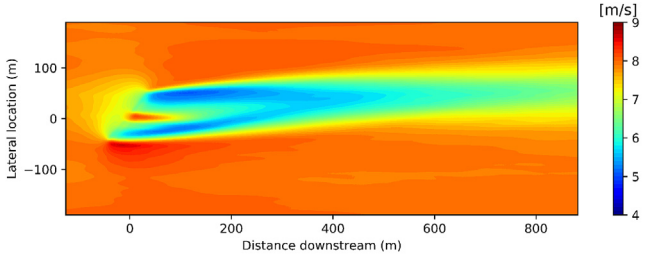

(a) Mean value predicted by SOWFA

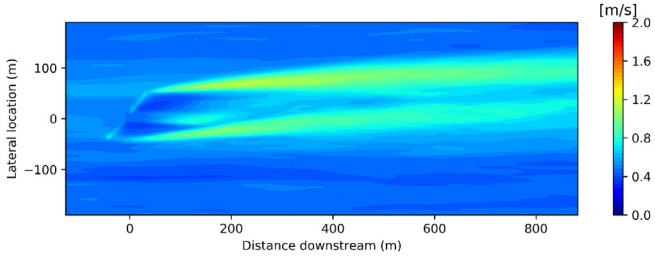

(b) Standard deviation predicted by SOWFA

Fig. 5. The prediction of the flow field by SOWFA for the case of turbine yaw equal to − 40°. The mean and standard deviation are calculated based on the instantaneous flow field from 400*s* to 900*s*.

Gaussian random variable:

$$\tilde{\mathbf{d}} = (1+\boldsymbol{\eta})\mathscr{M}(\mathbf{x},\mathbf{z}), \tag{2}$$

where $\tilde{\mathbf{d}}$ is the true value of the experimental observation, $\mathscr{M}(\mathbf{x},\mathbf{z})$ is the prediction of $\tilde{\mathbf{d}}$ by the computer model which depends on the explanatory variable $\mathbf{x}$ (e.g. turbine yaw angle) and the model parameter $\mathbf{z}$, and $\boldsymbol{\eta}$ is a random vector with each component η_i being zero-mean, independent and identically distributed Gaussian, i.e. $\eta_i \sim \mathscr{N}(0,\sigma^2)$. $\tilde{\mathbf{d}}$ can be related to the experimental observation $\mathbf{d}$ as:

$$\mathrm{d} = \tilde{\mathbf{d}} + \mathbf{e}. \tag{3}$$

Here $\mathbf{e}$ represents the measurement error, which is modeled as a zero mean, independent and identically distributed Gaussian, i.e. $e_i \sim \mathscr{N}(0,\sigma_e^2)$. σ_e is determined from the corresponding experiments. From Eqs. (2) and (3), the model output can be related to the experimental observation as

$$\mathrm{d} = (1+\boldsymbol{\eta})\mathscr{M}(\mathbf{x},\mathbf{z}) + \mathbf{e}. \tag{4}$$

Thus,

$$\mathrm{d}|\sigma,\mathbf{z} \sim \mathscr{N}(\boldsymbol{\mu},\boldsymbol{\lambda}), \tag{5}$$

where

$$\boldsymbol{\mu} = \mathscr{M}(\mathbf{x},\mathbf{z}) \text{ and } \boldsymbol{\lambda} = \mathscr{M}^T(\mathbf{x},\mathbf{z})\sigma^2\mathscr{M}(\mathbf{x},\mathbf{z}) + \sigma_e^2\boldsymbol{I}. \tag{6}$$

Eq. (1) can then be recast as:

$$p(\boldsymbol{\theta}_M|\mathbf{d}) \propto \frac{1}{\sqrt{(2\pi)^{N_d}|\boldsymbol{\lambda}|}} exp\left(-\frac{1}{2}\boldsymbol{\delta}^T\boldsymbol{\lambda}^{-1}\boldsymbol{\delta}\right)p(\boldsymbol{\theta}_M) \tag{7}$$

where $\boldsymbol{\theta}_M$ denotes $\{\sigma,\mathbf{z}\}$, N_d is the dimension of the experimental observation, $|\boldsymbol{\lambda}|$ represents the determinant of $\boldsymbol{\lambda}$, and $\boldsymbol{\delta} = \boldsymbol{d} - \mathscr{M}(\mathbf{x},\mathbf{z})$.

Then a sampler is employed to obtain the posterior samples according to Eq. (7) and the kernel estimation is used to evaluate the posterior PDFs of the model parameters. In this work the adaptive Metropolis-Hastings Markov chain Monte Carlo (MCMC) sampler [41], as implemented in the R [42] package MHadaptive [43], is employed. Once the calibration is completed, the model prediction can be carried out by propagating the posterior PDFs of model parameters through the computer model to obtain the PDFs of the QoIs. The so-obtained PDFs are in fact the posterior distribution of the QoIs given the experimental observation:

$$\begin{aligned} p(\tilde{\mathbf{q}}|\mathbf{d}) &= \int p(\tilde{\mathbf{q}},\mathbf{z}|\mathbf{d})d\mathbf{z} \\ &= \int p(\tilde{\mathbf{q}}|\mathbf{d},\mathbf{z})p(\mathbf{z}|\mathbf{d})d\mathbf{z} \\ &= \int p(\tilde{\mathbf{q}}|\mathbf{z})p(\mathbf{z}|\mathbf{d})d\mathbf{z}, \end{aligned} \tag{8}$$

where $\tilde{\mathbf{q}}$ represents the QoIs, which can be the same quantity as the experimental observation or other flow quantities. The last step in Eq. (2) follows by assuming $\tilde{\mathbf{q}}$ and $\mathbf{d}$ are conditionally independent given $\mathbf{z}$.

3. Application to wind farm wake modeling

The Bayesian UQ approach described above can be used for general fluid systems and is thus applied to wind farm wake

Table 2
The samples of turbine yaw angles generated by Latin Hypercube Sampling. γ_1 represents the front turbine yaw and γ_2 represents the rear turbine yaw.

Case No.	1	2	3	4	5	6	7	8	9	10	11	12	13	14	15
γ_1	16.5	0.1	12.7	2.3	−23.9	21.0	−6.7	−17.3	−3.1	−4.5	−14.1	−24.2	−14.0	8.1	24.4
γ_2	4.7	−1.0	24.8	8.7	−5.1	1.7	7.8	18.6	−21.8	21.2	−14.3	−26.4	−8.2	17.2	−2.6
continued	16	17	18	19	20	21	22	23	24	25	26	27	28	29	30
γ_1	−19.2	22.3	−9.6	−11.5	−28.4	28.6	15.4	6.7	−1.5	5.2	19.8	−27.3	27.5	−20.7	11.1
γ_2	−28.6	−19.4	−23.9	13.4	−17.0	−10.5	10.1	−24.2	28.0	−7.5	−13.9	14.9	3.1	27.0	22.6

modeling in this section. For this purpose, the computer model $\mathcal{M}(\mathbf{x},\mathbf{z})$ and the experimental observation $\mathbf{d}$ in Equation (7) need to be specified. Here the computer model $\mathcal{M}(\mathbf{x},\mathbf{z})$ is specified as the analytical wake model FLORIS, with $\mathbf{x}$ being the turbine yaw angle, $\mathbf{z}$ being the empirical parameters in FLORIS, and the output $\mathcal{M}$ being the flow field prediction. The detailed formulation of $\mathcal{M}(\mathbf{x},\mathbf{z})$ is given in Subsection 3.1. The experimental observation $\mathbf{d}$ is generated by high-fidelity numerical experiments with the simulation details given in Subsection 3.2.

3.1. An analytical wake model - FLORIS

The analytical wake model FLORIS is briefly described in this section, including the modeling of wake deflection, wake expansion and wake velocity. Further details can be found in Ref. [14].

For wake deflection, the turbine wake center $y_w(x)$ is determined by

$$y_w(x) = Y + \delta y_{w,rotation}(x) + \delta y_{w,yaw}(x), \tag{9}$$

where x is the downwind coordinate, Y is the turbine's crosswind location, and $\delta y_{w,rotation}(x)$ and $\delta y_{w,yaw}(x)$ represent the rotation-induced and yaw-induced wake lateral offset. They are formulated as:

$$\delta y_{w,rotation}(x) = a_d + b_d[x - X], \tag{10}$$

and

$$\delta y_{w,yaw}(x) = \frac{\xi_{init}(a,\gamma)\left[15\left[\frac{2k_d[x-X]}{D}+1\right]^4 + \xi_{init}(a,\gamma)^2\right]}{\frac{30k_d}{D}\left[\frac{2k_d[x-X]}{D}+1\right]^5} \tag{11}$$

$$-\frac{\xi_{init}(a,\gamma)D\left[15+\xi_{init}(a,\gamma)^2\right]}{30k_d}, \tag{12}$$

where X is the turbine's downwind location, D is the turbine rotor diameter, a is the axial induction factor, γ is the yaw angle, and $\xi_{init}(a,\gamma) = 2cos^2(\gamma)sin(\gamma)a[1-a]$. Three empirical parameters, a_d, b_d, and k_d, are involved in this deflection model. After determining the center of the wake location, the wake region behind the turbine is divided into three zones and the diameters of each zone are given by

$$D_{w,q}(x) = max\left(D + 2k_e m_{e,q}[x - X], 0\right), x > X, \tag{13}$$

where the index q represents the different zones. The three zones are the "near wake" ($q = 1$), "far wake" ($q = 2$), and "mixing zone"($q = 3$). k_e, $m_{e,1}$, $m_{e,2}$ and $m_{e,3}$ are the four empirical parameters involved in this wake expansion model. The velocity profile within zone q is then modeled as

$$U_{w,q}(x) = U\left[1 - 2ac_q(x)\right] \tag{14}$$

where U is the freestream wind speed, and

$$c_q(x) = \left[\frac{D}{D + 2k_e[x - X]M_{U,q}/cos(a_U + b_U\gamma)}\right]^2. \tag{15}$$

Five empirical parameters, a_U, b_U, $M_{U,1}$, $M_{U,2}$, and $M_{U,3}$, are used in calculating the wake profile. From the formulation above, it can be seen that the FLORIS model predicts the velocity profile at a specific downwind location as a piecewise constant function.

In total, there are 12 empirical model parameters in the FLORIS model. For Bayesian calibration, the prior distributions of these parameters, i.e. p($\mathbf{z}$), need to be specified. In this work, the uniform distribution is used and their prior ranges are given in Table 1. They are determined by trial and error and are kept as large as possible so that the posterior is mainly determined by the likelihood.

3.2. High-fidelity data generation

SOWFA is employed here to generate high-fidelity CFD data for Bayesian calibration of the FLORIS model described in Subsection 3.1. SOWFA is a numerical solver developed based on OpenFOAM for the 3D large eddy simulation of wind flow around wind turbine array in the atmospheric boundary layer, where the turbine rotors are represented by actuator disk model (ADM) or actuator line model (ALM). The detailed implementations and validations of SOWFA can be found in Refs. [13,40]. First, a precursor simulation of neutral atmospheric boundary layer is carried out to obtain the initial flow field and inflow boundary conditions. The employed turbulent inflow has a mean hub-height free-stream wind velocity of around $8m/s$ and a free-stream turbulence intensity (FSTI) of 6%. For the subsequent wind farm simulations, wind turbines are modeled using ALM and the baseline pitch and torque control are defined as in Ref. [44]. A top view of the simulation domain at hub height is shown in Fig. 1. The size of the simulation domain is $3000m \times 3000m \times 1000m$, with the inflow wind coming from southwest direction. For the mesh generation, a two-level local mesh refinement is used, as is suggested in Ref. [45]. The outer mesh dimension is $12m \times 12m \times 12m$, the inner mesh dimension is $3m \times 3m \times 3m$, and the dimension of the mesh in-between is $6m \times 6m \times 6m$. The total number of cells is 1.8×10^7. In this way, the mesh size around the turbine rotors is 3 m so that the simulation can capture the detailed turbine wake dynamics. A NREL 5-MW baseline turbine is positioned in the simulation domain. For each turbine yaw angle, 1000-s simulations are carried out with a time step of $0.02s$. The mean velocity field is then obtained by averaging the instantaneous flow field from $400s$ to $900s$. Each high-fidelity simulation by SOWFA requires around 30 h using 256 processors. The generated LES data is then used to carry out the Bayesian calibration in the next section.

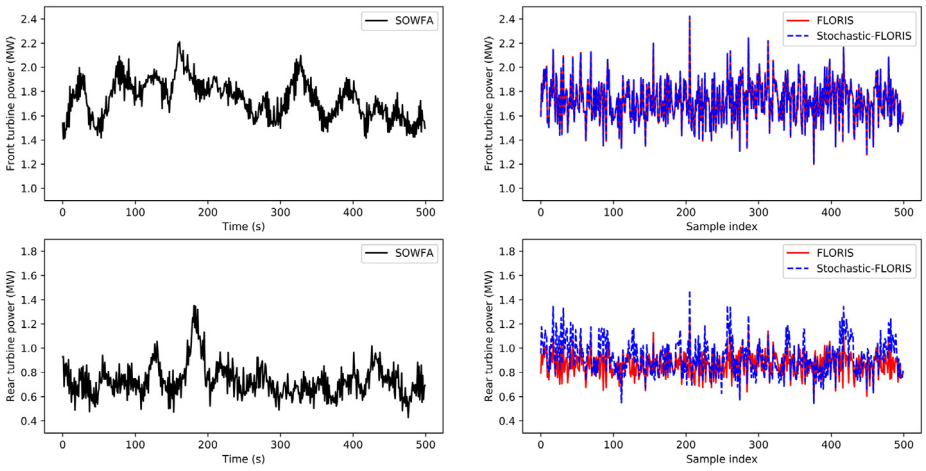

(a) $\gamma_1 = 0.1°, \gamma_2 = -1.0°$

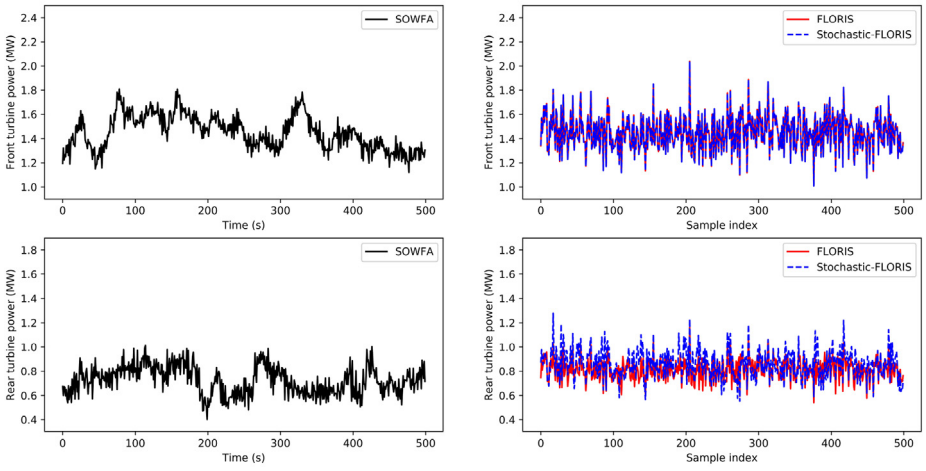

(b) $\gamma_1 = -24.2°, \gamma_2 = -26.4°$

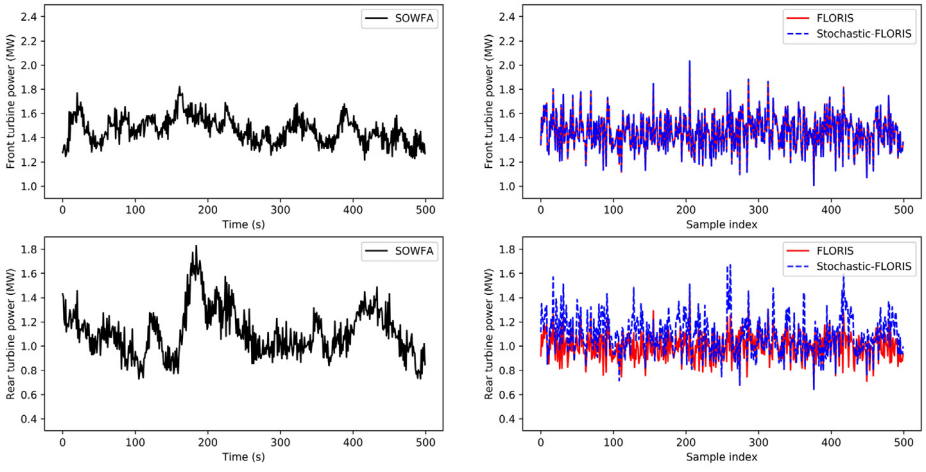

(c) $\gamma_1 = 24.4°, \gamma_2 = -2.6°$

Fig. 6. The time series of power generation predicted by SOWFA and the trace of the power samples predicted by FLORIS/Stochastic-FLORIS. Three cases with different yaw angles are included.

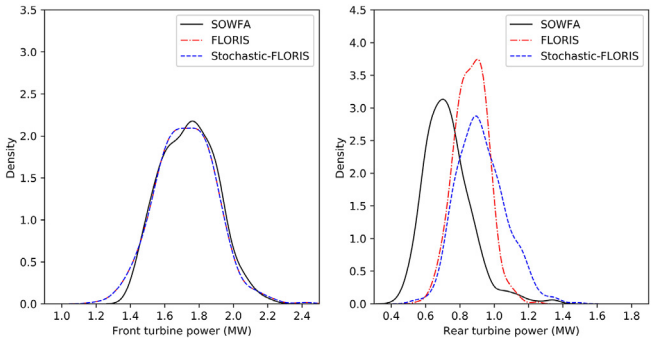

(a) $\gamma_1 = 0.1°, \gamma_2 = -1.0°$

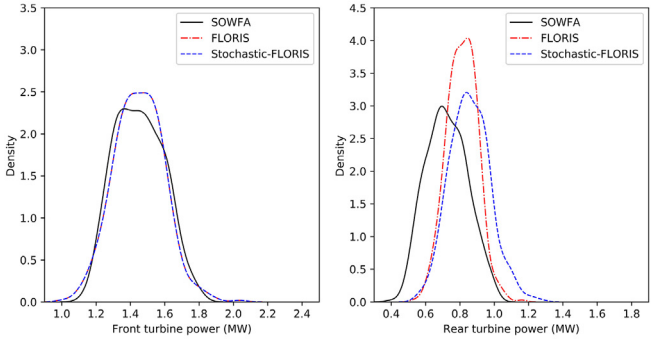

(b) $\gamma_1 = -24.2°, \gamma_2 = -26.4°$

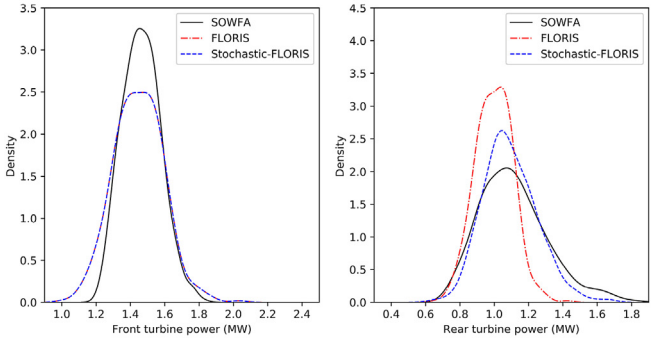

(c) $\gamma_1 = 24.4°, \gamma_2 = -2.6°$

Fig. 7. The distribution of power generation predicted by SOWFA, FLORIS, and Stochastic-FLORIS. Three cases with different yaw angles are included.

4. Results

4.1. Model calibration

In order to calculate the likelihood, the stochastic model is constructed according to Section 2. Since the parameter uncertainty is the main focus of the current investigation, the model inadequacy term is ignored in the remaining part of this paper. SOWFA is employed for generating high-fidelity flow field data for three scenarios, i.e. $\gamma = -40°$, $\gamma = 0°$, and $\gamma = 40°$. Then the hub-height velocity profile at 5 rotor diameters downstream behind the wind turbine is extracted to calibrate the FLORIS model, as the wind farm with downwind spacing of 5 rotor diameters is of great practical interests and has been studied previously for wake modeling and wind farm control [14]. The measurement error is estimated as the zero-mean Gaussian with $\sigma_e = \text{FSTI} \times U_\infty$. 12000 MCMC samples of the model parameters are generated with a burn-in length set to 2000. The kernel estimation is used to estimate the posterior PDF from the MCMC samples. The results are shown in Fig. 2. For simplicity, the posterior distributions of the model parameters arising from modeling wake deflection, wake expansion and wake velocity are shown in different sub-figures. As can be seen from Fig. 2, most of the model parameters are well identified. Among them, the correlation between a_d and b_d is strong, which agrees with the design of the wake deflection. In fact, both parameters intend to capture the same aspect of the wake flow, i.e., the rotation-induced lateral offset of the turbine wake. The nominal values of the model parameters reported in Ref. [14] are also shown in Fig. 2. They are the optimal values determined by matching the turbine power with the SOWFA results for a wind farm with 7 rotor diameters' downwind spacing. The Maximum A Posteriori (MAP) values of our calibration are slightly different from their reported values, which is reasonable as the downwind spacing of our calibration case (5 rotor diameters) is slightly different from theirs.

The posterior model check is then carried out by propagating the posterior PDFs of the model parameters through the FLORIS model. The predictions with quantified uncertainty for the velocity profiles at 5 rotor diameters downstream are shown in Fig. 3. The results with nominal and MAP model parameters are also shown for comparison. As can be seen, the predicted velocity profile with quantified uncertainty matches well with SOWFA results, indicating the Bayesian calibration is done successfully. In addition, since the FLORIS model divides the wake into three distinct zone and the velocity is determined separately in each zone as a constant function of the crosswind coordinate y, the velocity profile predicted with nominal/MAP model parameters is discontinuous at the zone boundary, while in reality the wake dynamics should be continuous. In this sense, the predicted mean value of the velocity profile matches much better with SOWFA results than the nominal/MAP predictions.

4.2. Evaluation of the stochastic FLORIS model

After model calibration, the FLORIS model with its parameters specified by their posterior distributions can be used to predict the statistics of the flow field, turbine power generation, turbine torque, etc. Hereby the FLORIS with uncertain model parameters is denoted as the stochastic FLORIS model and we evaluate the stochastic FLORIS model's performance in terms of predicting wind farm flow field and turbine power generation in this section.

4.2.1. Flow field prediction

The posterior distributions of the 2D flow field at hub height are obtained by propagating the PDFs of the model parameters through FLORIS model. The mean value and standard deviation of the flow field are given in Fig. 4 for the case of turbine yaw equal to $-40°$. The analysis for $0°$ and $40°$ turbine yaws are similar, thus omitted. For comparison, the FLORIS prediction with MAP model parameters is also included in Fig. 4. The mean and standard deviation of the unsteady SOWFA results are given in Fig. 5. As can be seen, the mean flow field given by stochastic FLORIS matches better with SOWFA than the MAP results. Furthermore, the standard deviation of SOWFA and stochastic FLORIS results shares a similar qualitative feature: the largest unsteadiness/uncertainty is in the "mixing zone".

4.2.2. Turbine power generation prediction

In order to evaluate the stochastic FLORIS model's performance in predicting turbine power generations, a series of high-fidelity simulations are carried out for the case of two turbines operating in a row. The simulation domain and mesh configuration of these

two-turbine cases are the same as the one-turbine cases shown in Fig. 1. The only difference is that another NREL 5-MW turbine is added in the flow domain located at 5 rotor diameter downstream of the first turbine. 30 samples of turbine yaw angles are generated by Latin Hypercube Sampling and the yaw angles are reported in Table 2. SOWFA is then employed to generate the high-fidelity data for the 30 cases and each SOWFA simulation requires around 30 h using 256 processors. The turbine power generation is recorded for the simulation period of 500 s (from 400s to 900s). The turbine power generation is one of the primary concerns in wind farm design and control, thus we now focus on the evaluation of FLORIS and stochastic FLORIS in terms of predicting turbine power generation.

In order to obtain a better prediction of the turbine power generations, the input (inflow wind speed) uncertainty is also considered in the FLORIS and stochstic FLORIS prediction. We simply assume the inflow wind speed as a Gaussian, i.e. $u_\infty \sim \mathcal{N}(\mu_u, \sigma_u^2)$ ($\mu_u = 7.83$ and $\sigma_u = 0.276$). The mean value and the standard deviation are estimated from the unsteady inflow boundary condition of SOWFA simulations so that all the predictions are carried out with the same inflow wind condition.

First, we compare the time series of power generation predicted by SOWFA and the trace of the power samples predicted by FLORIS. Three typical cases are shown in Fig. 6, where the front turbine is in the condition of no yaw, negative yaw, and positive yaw respectively. The results predicted by FLORIS with MAP model parameters and stochastic FLORIS are both included. For all three cases, FLORIS and stochastic FLORIS get the same results for predictions of power generations of the front turbine, as the inclusion of parameter uncertainty only introduces uncertainty to the downstream wake flow (thus only affecting the rear turbine's power generation). For the rear turbine, stochastic FLORIS predicts similar power fluctuations as the ones given by SOWFA, while FLORIS with only input uncertainty predicts much smaller power fluctuations. However, it should be noted that this comparison is only meaningful in statistical sense, because the trace of power samples of FLORIS do not have time relevance. In addition, the turbine power distributions can also be obtained from the time-series data or statistical samples, which are shown in Fig. 7. It is clear that stochastic FLORIS results match with SOWFA results much better than FLORIS. The FLORIS can be employed as an internal model for wind farm control to maximise the power generation, e.g. in Ref. [14]. Because the stochastic FLORIS can predict the distribution of power generation, it can be used for more purposes, such as maximising the average power, minimizing the power fluctuation, guaranteeing certain amount of power generation with certain confidence level, etc.

To further evaluate the performance of the stochastic FLORIS model, the predictions of turbine average powers and power fluctuations for all the 30 cases are given in Figs. 8 and 9. The FLORIS and stochastic FLORIS get same results for the power predictions of the front turbine. They differ slightly in the predictions of rear turbine's average power, and their performances are similar compared to SOWFA results. However, compared with FLORIS, the power fluctuation prediction ability of the stochastic FLORIS is improved dramatically in all the 30 cases due to the inclusion of parameter uncertainty.

5. Conclusions

The parameter uncertainty of FLORIS model has been investigated in this work. Large eddy simulations (LES) of wind farms were carried out with different turbine yaw angles and the generated high-fidelity flow field data was used to infer the model parameters. After model calibration, the posterior model check showed that the predicted mean velocity profile with the quantified uncertainty matched well with the high-fidelity LES data. The

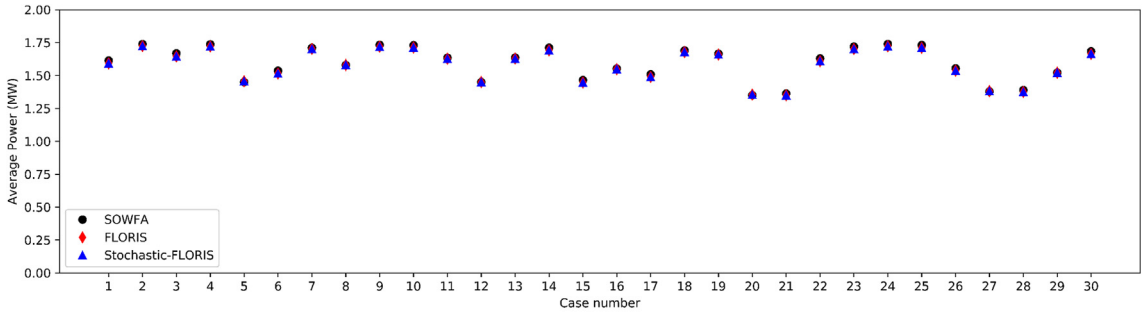

(a) Power generation average value

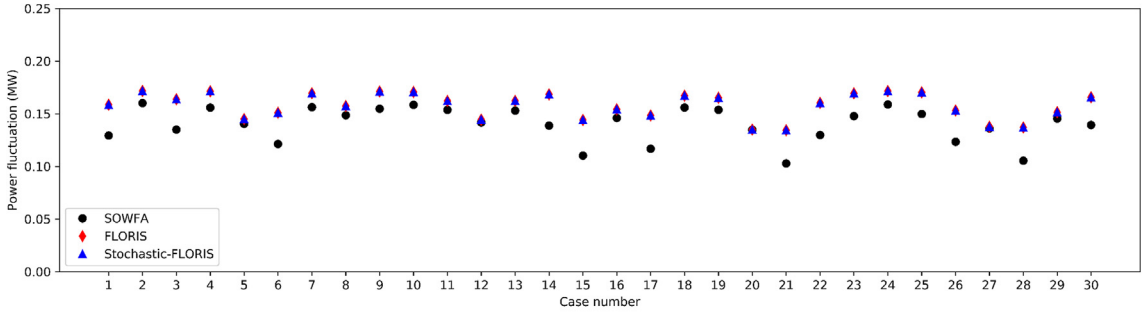

(b) Power generation standard deviation

Fig. 8. Front turbine power generation predicted by SOWFA, FLORIS, and Stochastic-FLORIS.

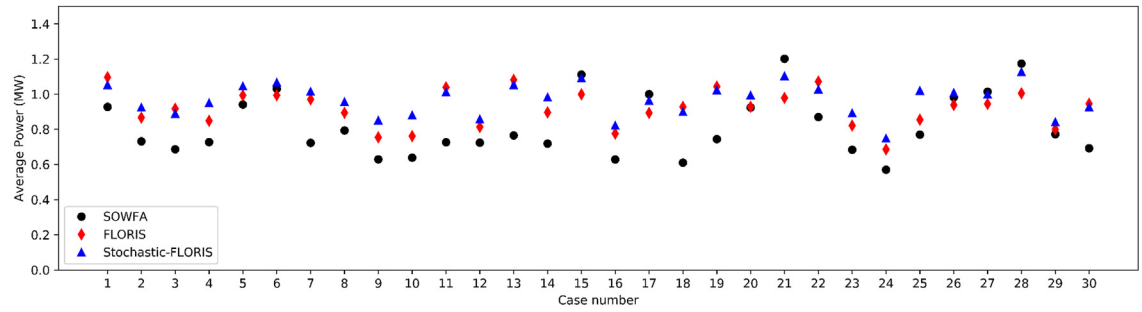

(a) Power generation average value

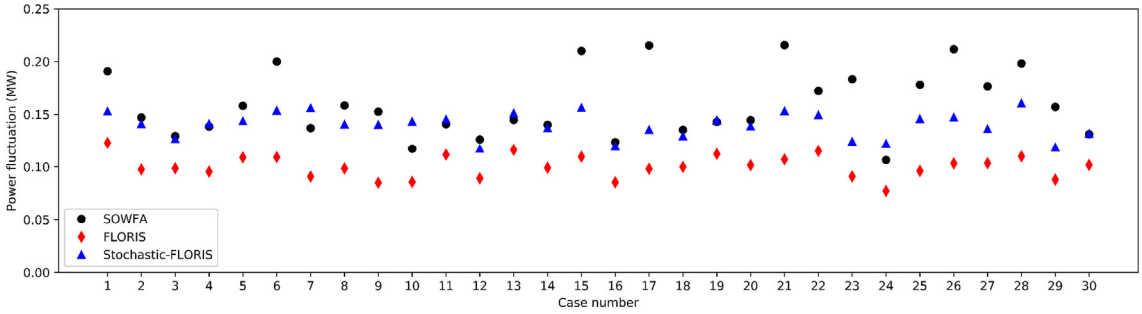

(b) Power generation standard deviation

Fig. 9. Rear turbine power generation predicted by SOWFA, FLORIS, and Stochastic-FLORIS.

prediction of other wind farm quantities, such as the hub-height flow field and the turbine power generation, was then carried out. The results showed that the inclusion of parameter uncertainty improved the flow field prediction and a correct characteristic of uncertainty in the "mixing zone" was predicted, which agreed with the high-fidelity SOWFA results. As for the power generation, the inflow wind speed uncertainty was also included and the stochastic FLORIS performed similarly as the FLORIS model in terms of predicting average turbine power, but it performed much better in terms of predicting the turbine power fluctuation in all the test cases. This meant that the stochastic FLORIS model can be used to not only maximise the average power but also minimise the power fluctuation.

Future research may involve the UQ of other wake models in order to reveal further insight in wake modeling and to improve the reliability of wind farm wake predictions. Another important research direction is the application of the resulting stochastic wake model in wind farm optimal design and control. In order to facilitate the use of the stochastic FLORIS model for wind farm design and control community, the MCMC samples of the model parameters are reported in the supporting material of this paper. It can be used directly with FLORIS for predicting the statistics of the turbine power generation, turbine torque, flow field, etc.

Acknowledgments

This research has received funding from the European Union's Horizon 2020 research and innovation programme under the Marie Sklodowska-Curie grant agreement No 765579. The authors acknowledge the Scientific Computing Research Technology Platform (SCRTP) at University of Warwick for providing high performance computing resources. They also acknowledge the support of the UK Engineering and Physical Sciences Research Council (grant number: EP/R007470/1).

Appendix A. Supplementary data

Supplementary data to this article can be found online at https://doi.org/10.1016/j.energy.2020.117065.

References

[1] Adaramola M, Krogstad P-Å. Experimental investigation of wake effects on wind turbine performance. Renew Energy 2011;36(8):2078–86.
[2] Gao X, Yang H, Lu L. Optimization of wind turbine layout position in a wind farm using a newly-developed two-dimensional wake model. Appl. Energy 2016;174:192–200.
[3] Yang K, Kwak G, Cho K, Huh J. Wind farm layout optimization for wake effect uniformity. Energy 2019;183:983–95.
[4] Boersma S, Doekemeijer B, Gebraad PM, Fleming PA, Annoni J, Scholbrock AK, Frederik J, van Wingerden J-W. A tutorial on control-oriented modeling and control of wind farms. In: 2017 American control conference. IEEE: ACC); 2017. p. 1–18.
[5] Martínez-Tossas LA, Churchfield MJ, Leonardi S. Large eddy simulations of the flow past wind turbines: actuator line and disk modeling. Wind Energy 2015;18(6):1047–60.
[6] Witha B, Steinfeld G, Heinemann D. High-resolution offshore wake simulations with the les model palm. In: Wind energy-impact of turbulence. Springer; 2014. p. 175–81.
[7] Larsen GC, Aagaard HM, Bingöl F, Mann J, Ott S, Sørensen JN, Okulov V, Troldborg N, Nielsen NM, Thomsen K, et al. Dynamic wake meandering modeling. 2007.
[8] Boersma S, Doekemeijer B, Vali M, Meyers J, Wingerden J-W v. A control-oriented dynamic wind farm model: Wfsim. Wind Energy Sci. 2018;3(1):75–95.
[9] Jensen NO. A note on wind generator interaction. 1983.
[10] Katic I, Højstrup J, Jensen NO. A simple model for cluster efficiency. In: European wind energy association conference and exhibition. A. Raguzzi; 1987.
[11] Frandsen S, Barthelmie R, Pryor S, Rathmann O, Larsen S, Højstrup J, Thøgersen M. Analytical modelling of wind speed deficit in large offshore wind farms. Wind Energy: Int. J. Progress and Appl. Wind Power Conversion Technol. 2006;9(1–2):39–53.
[12] Lu H, Porté-Agel F. Large-eddy simulation of a very large wind farm in a stable atmospheric boundary layer. Phys Fluids 2011;23(6):065101.
[13] Churchfield MJ, Lee S, Michalakes J, Moriarty PJ. A numerical study of the effects of atmospheric and wake turbulence on wind turbine dynamics. J Turbul 2012;13:N14.
[14] Gebraad P, Teeuwisse F, Van Wingerden J, Fleming PA, Ruben S, Marden J,

Pao L. Wind plant power optimization through yaw control using a parametric model for wake effects—a cfd simulation study. Wind Energy 2016;19(1):95—114.
[15] Calaf M, Meneveau C, Meyers J. Large eddy simulation study of fully developed wind-turbine array boundary layers. Physics of fluids 2010;22(1):015110.
[16] Meyers J, Meneveau C. Large eddy simulations of large wind-turbine arrays in the atmospheric boundary layer. In: 48th AIAA aerospace sciences meeting including the new horizons forum and aerospace exposition; 2010. p. 827.
[17] Nilsson K, Ivanell S, Hansen KS, Mikkelsen R, Sørensen JN, Breton S-P, Henningson D. Large-eddy simulations of the lillgrund wind farm. Wind Energy 2015;18(3):449—67.
[18] Wu Y-T, Porté-Agel F. Modeling turbine wakes and power losses within a wind farm using les: an application to the horns rev offshore wind farm. Renew Energy 2015;75:945—55.
[19] Bastankhah M, Porté-Agel F. A new analytical model for wind-turbine wakes. Renew Energy 2014;70:116—23.
[20] Tian L, Zhu W, Shen W, Zhao N, Shen Z. Development and validation of a new two-dimensional wake model for wind turbine wakes. J Wind Eng Ind Aerod 2015;137:90—9.
[21] Niayifar A, Porté-Agel F. Analytical modeling of wind farms: a new approach for power prediction. Energies 2016;9(9):741.
[22] Lopez D, Kuo J, Li N. A novel wake model for yawed wind turbines. Energy 2019;178:158—67.
[23] Ge M, Wu Y, Liu Y, Li Q. A two-dimensional model based on the expansion of physical wake boundary for wind-turbine wakes. Appl. energy 2019;233:975—84.
[24] Sun H, Gao X, Yang H. Validations of three-dimensional wake models with the wind field measurements in complex terrain. Energy 2019;189:116213.
[25] Kabir IFSA, Safiyullah F, Ng E, Tam VW. New analytical wake models based on artificial intelligence and rivalling the benchmark full-rotor cfd predictions under both uniform and abl inflows. Energy 2019:116761.
[26] Böhme GS, Fadigas EA, Gimenes AL, Tassinari CE. Wake effect measurement in complex terrain-a case study in brazilian wind farms. Energy 2018;161:277—83.
[27] Gaumond M, Réthoré P-E, Ott S, Pena A, Bechmann A, Hansen KS. Evaluation of the wind direction uncertainty and its impact on wake modeling at the horns rev offshore wind farm. Wind Energy 2014;17(8):1169—78.
[28] Peña A, Réthoré P-E, van der Laan MP. On the application of the jensen wake model using a turbulence-dependent wake decay coefficient: the sexbierum case. Wind Energy 2016;19(4):763—76.
[29] Quick J, Annoni J, King R, Dykes K, Fleming P, Ning A. Optimization under uncertainty for wake steering strategies. Journal of Physics: Conference series, vol. 854. IOP Publishing; 2017, 012036.
[30] Rott A, Doekemeijer B, Seifert JK, Wingerden J-W v, Kühn M. Robust active wake control in consideration of wind direction variability and uncertainty. Wind Energy Sci. 2018;3(2):869—82.
[31] Kennedy MC, O'Hagan A. Bayesian calibration of computer models. J Roy Stat Soc B 2001;63(3):425—64.
[32] Cheung SH, Oliver TA, Prudencio EE, Prudhomme S, Moser RD. Bayesian uncertainty analysis with applications to turbulence modeling. Reliab Eng Syst Saf 2011;96(9):1137—49.
[33] Edeling W, Cinnella P, Dwight RP, Bijl H. Bayesian estimates of parameter variability in the k—ε turbulence model. J Comput Phys 2014;258:73—94.
[34] Zhang J, Fu S. An efficient approach for quantifying parameter uncertainty in the sst turbulence model. Comput. Fluids 2019;181:173—87.
[35] Oliver TA, Moser RD. Bayesian uncertainty quantification applied to rans turbulence models. In: Journal of Physics: Conference series, vol. 318. IOP Publishing; 2011, 042032.
[36] Zhang J, Fu S. An efficient bayesian uncertainty quantification approach with application to k-ω-γ transition modeling. Comput. Fluids 2018;161:211—24.
[37] Ray J, Lefantzi S, Arunajatesan S, Dechant L. Bayesian parameter estimation of ak-ε model for accurate jet-in-crossflow simulations. AIAA J 2016:2432—48.
[38] Doekemeijer BM, Van Wingerden J-W, Fleming PA. A tutorial on the synthesis and validation of a closed-loop wind farm controller using a steady-state surrogate model. In: 2019 American control conference. IEEE: ACC); 2019. p. 2825—36.
[39] Nwtc Information Portal (Sowfa). https://nwtc.nrel.gov/SOWFA.
[40] Churchfield M, Lee S, Moriarty P, Martinez L, Leonardi S, Vijayakumar G, Brasseur J. A large-eddy simulation of wind-plant aerodynamics. In: 50th AIAA aerospace sciences meeting including the new horizons forum and aerospace exposition; 2012. p. 537.
[41] Haario H, Saksman E, Tamminen J, et al. An adaptive metropolis algorithm. Bernoulli 2001;7(2):223—42.
[42] Team RC, R, et al. A language and environment for statistical computing. 2013.
[43] Chivers C. Mhadaptive: general Markov chain Monte Carlo for bayesian inference using adaptive metropolis-hastings sampling. 2012.
[44] Jonkman J, Butterfield S, Musial W, Scott G. Definition of a 5-mw reference wind turbine for offshore system development, Tech. rep.. Golden, CO (United States): National Renewable Energy Lab.(NREL); 2009.
[45] Fleming P, Gebraad PM, Lee S, van Wingerden J-W, Johnson K, Churchfield M, Michalakes J, Spalart P, Moriarty P. Simulation comparison of wake mitigation control strategies for a two-turbine case. Wind Energy 2015;18(12):2135—43.